

Analysis of two-dimensional photonic band gaps of any rod shape and conductivity using a conical-integral-equation method

Leonid I. Goray*

Saint Petersburg Academic University, Khlopina 8/3, St. Petersburg 194021, and Institute for Analytical Instrumentation, RAS, Rizhsky Prospect 26, St. Petersburg 190103, Russian Federation

Gunther Schmidt

Weierstrass Institute of Applied Analysis and Stochastics, Mohrenstr. 39, D-10117 Berlin, Germany
(Received 28 October 2011; revised manuscript received 14 January 2012; published 5 March 2012)

The conical-boundary-integral-equation method has been proposed for calculation of the sensitive optical response of two-dimensional photonic band gaps (PBGs), including dielectric, absorbing, and high-conductive rods of various shapes working in any wavelength range. It is possible to determine the diffracted field by computing the scattering matrices separately for any grating boundary profile. The computation of the matrices is based on the solution of a 2×2 system of singular integral equations at each interface between two different materials. The advantage of our integral formulation is that the discretization of the integral equation system and the factorization of the discrete matrices, which takes the majority of the computing time, are carried out only once for a boundary. It turns out that a small number of collocation points per boundary combined with a high convergence rate can provide an adequate description of the dependence on diffracted energy of very different PBGs illuminated at arbitrary incident and polarization angles. The numerical results presented describe the significant impact of rod shape on diffraction in PBGs supporting polariton-plasmon excitation, particularly in the vicinity of resonances and at high filling ratios. The diffracted energy response calculated vs the array cell geometry parameters was found to vary from a few up to a few hundred percent. The influence of other types of anomalies (i.e., waveguide anomalies, cavity modes, Fabry-Perot and Bragg resonances, Rayleigh orders, etc.), conductivity, and polarization states on the optical response is demonstrated.

DOI: [10.1103/PhysRevE.85.036701](https://doi.org/10.1103/PhysRevE.85.036701)

PACS number(s): 02.60.Nm, 02.70.Pt, 71.36.+c

I. INTRODUCTION

In the past two decades, we have been witnessing exponentially growing interest, of both theoreticians and experimenters, in the properties of photonic band gaps (PBGs) and metamaterials. Progress in the technology of nanostructures with a characteristic surface relief size of the order of 10–100 nm has stimulated production of two- and three-dimensional (2D and 3D) periodic structures with periods shorter than the wavelength λ of visible light, i.e., subwavelength diffraction gratings. Nowadays considerable effort is devoted to the investigation of polariton-plasmon PBGs with metallic or semiconducting nanostructures supporting strong light-matter interaction. Large PBGs, extraordinary light transmission properties, negative refraction, and strong coupling between electronic and photonic resonances can be supported in such structures. Though surface plasmon excitation plays a predominant part in metallic subwavelength PBGs, other types of electromagnetic resonances can also exist in complex material structures working in different wavelength ranges: Rayleigh anomalies, Fabry-Perot and Bragg resonances, waveguiding anomalies, cavity modes, etc. In some cases it is difficult to distinguish among these phenomena, owing to their gradual mutation from one into another, and determine which is which, even using electromagnetic field map distributions inside the slab structure. There is therefore

a growing need for methods based on a rigorous theory which would be universal, accurate, and fast enough.

Numerical methods are ordinarily employed in treating diffracting structures whose characteristic dimensions [more specifically, period d , slab (rod) width l , depth h , correlation length, etc.] are comparable with the wavelength of the incident radiation ($\lambda/d \sim 1$), i.e., in the resonance region. Structures with subwavelength dimensions require solution of the problem in terms of electromagnetic theory, in other words, of Maxwell's equations with rigorous boundary conditions and radiation conditions [1]. A wide range of various techniques that have been developed for the analysis of some kinds of gratings may also be used for PBG analysis [2]. Theory offers presently rigorous numerical methods to solve problems of diffraction from multiboundary one-dimensional (1D) and 2D gratings with arbitrary groove profiles, which can conveniently be assigned to two branches, integral or differential, of electromagnetic theory. The first of these includes, again, by convention only, methods involving finite elements (including boundary or volume, time, or frequency domain), fictitious sources, and integral equations (boundary or volume). Some methods closely resembling the differential approach, among them the modal (sometimes referred to as characteristic-wave or characteristic-modal) method, coupled-wave (Fourier-modal) method, and method of coordinate transformation, are classified by some researchers among a special group [3,4]. They are all based essentially on Maxwell's equations in partial derivatives. In the general case, differential theory typically includes integration of these equations over one or two coordinates. Most of the currently used differential

*lig@pcgrate.com; also at I.I.G., Inc., P.O. Box 131611, Staten Island, New York 10313, USA.

methods resort to 1D integration or some other numerical approach in solving a system of conventional differential equations. The method of boundary integral equations (briefly, IM) treats Maxwell's equations in the integrodifferential form, with their subsequent numerical solution by curvilinear integration. Some versions of the finite-element method can also be assigned to the integral theory. In contrast to the method of integral equations, this approach assumes, as a rule, 2D integration, the only exclusion being the method of boundary integral elements. Drawing basically close to the method of integral equations is that of fictitious sources [2]. For a comprehensive review of a large number of theoretical treatments and their mathematical realizations, the reader is referred to the above-mentioned books and references therein.

The approach most frequently followed when considering scattering from ordered or partially ordered objects like PBGs is the straightforward and readily tractable plane-wave expansion method [5]. Although a plethora of more or less universal and effective rigorous analyses exists, this is a good introduction to the business of band diagrams and is probably the easiest method to understand [6]. It is well known that this method suffers from poor convergence for metallic gratings and needs large computation times, especially for transverse magnetic (TM)-polarized incident light, because of its main accuracy parameter scaling cubically with time [7,8]. In the theoretical investigations applied to diffraction gratings this approach is well known as the rigorous coupled-wave analysis (CWA). We dwell on it in some detail to be able to compare its advantages and shortcomings with the IM employed by the present authors in treating PBGs and other grating problems.

In many problems of diffraction monochromatic light is used and analysis of these problems requires solution of the scalar or vector Helmholtz equation (in its wave form). If we restrict ourselves to consideration of periodic objects only, for example, to 1D or 2D diffraction gratings and 2D or 3D photonic crystals, the CWA will turn out to be particularly appropriate for operation with the Helmholtz equation. The first to apply it, albeit not in a rigorous formulation, to analysis of volume holograms was Kogelnik, as far back as 1969. M. Moharam and T. Gaylord applied the coupled-wave method to analysis of diffraction gratings in its rigorous formulation, at any rate, to gratings with a lamellar (rectangular) profile in 1981 [9]. The CWA treats the electromagnetic field $u(x, y)$ in homogeneous regions of space, in front of a periodic object and behind it, as being comprised of a linear combination of plane waves. For a nonperiodic confined object, one has to accept, in place of a linear combination of plane waves, a continuous expansion in plane waves in the form of the Fourier integral. In the region of the object, Maxwell's equations are solved by Fourier transformation. To find the unknown coefficients in the Fourier expansions, a system of linear algebraic equations is formulated. Application of the CWA to classical 2D diffraction problems with 1D-periodic boundaries, i.e., with a stepwise changing dielectric and/or magnetic permeability at the boundary, is essentially different for the transverse electric (TE) and TM cases (with the electric vector either confined to the plane perpendicular to the plane of the incident wave vector \mathbf{k} and parallel to the grating grooves or lying in the \mathbf{k} plane,

respectively). In the case of TE polarization, the unknown electromagnetic field and its normal derivative remain continuous at the boundary. For TM polarization, the normal derivative suffers a discontinuity, which is responsible for all subsequent problems associated with the convergence and accuracy of the method, an issue that nobody has yet found a way to combat. While the CWA intuitively appears to be tractable, the present authors are unaware of any mathematical publications which offer a rigorous substantiation of its convergence, even for a smooth wave-number $k(x, y)$ relation. The main difficulty standing in the way of such a substantiation is the exponential growth of the elements of transmission matrices along the rows and columns [4]. This growth gives rise to numerical problems; matrices and the corresponding systems of differential equations are poorly conditioned; indeed, their eigenvalues belong to different scales, and this effect is stronger the more harmonics are taken into account [10]. Obviously enough, diffraction problems with a discontinuity of k at the interfaces will meet with the natural constraint on the convergence rate for the CWA. Indeed, the Fourier coefficients of $k^2(x, y)$ and $u(x, y)$ cannot approach 0 fast enough for the $y = \text{const.}$ line which crosses the boundary. The best version of factorization available thus far for the CWA and other similar methods of the differential group in TM polarization, called the fast Fourier factorization method [4], presently enjoys wide recognition. Its authors have, however, revealed the remaining above-mentioned limitations of a fundamental nature, which place a constraint on the use of this approach in cases of high conductivity in TM polarization [11]. In addition to the fast Fourier factorization method, a lot of other substantial improvements in the CWA have been introduced by various authors during the last decade (see, e.g., Ref. [12]). Despite the more stable and robust formulations presented in these publications, good convergence of numerical examples in TM polarization has been demonstrated for metallic lamellar gratings with a permittivity real part not less than -10^2 , which corresponds to the near-infrared spectral region. Metals in the medium-infrared, far-infrared, terahertz, and microwave regions have smaller permittivity real parts, up to orders of magnitude, however, the perfect conductivity model cannot be applied to modern PBG and waveguide structures. Besides, application of the CAW to nonlamellar profiled gratings involves discretization into plane layers, the so-called staircase approximation. This approximation was shown not to be rigorous [13]; indeed, as the number of layers increases, the result obtained in solution of the equations will not necessarily tend to accurate values. In the case of TE polarization and 1D gratings, the convergence of this approximation is, as a rule, good, but in the TM case an increase in the number of layers does not improve the results; on the contrary, they begin to diverge. This can also be seen from an analysis of the properties of the solution in the case of one boundary and TM polarization [14]. The conclusions drawn for the case of 2D diffraction from 1D gratings with one boundary will naturally hold for multiboundary gratings, conical (3D) diffraction, and biperiodic gratings. Nevertheless, for lack of a better alternative, the CWA is widely used for 1D and 2D gratings in micro-optics analysis and waveguide technology, as well as in problems involving synthesis, for instance, of

multiorder diffraction gratings or diffraction optical elements with preset characteristics [15].

The IM is presently universally recognized as one of the most developed and flexible approaches to accurate numerical solution of diffraction grating problems (cf. Refs. [1,16,17] and references therein). Viewed in the historical context, this method was the first to offer a solution to vector problems of light diffraction by optical gratings with a high enough accuracy and to demonstrate remarkable agreement with experimental data [3,18]. This should be attributed to the high accuracy and good convergence of the method, especially for the TM polarization plane [17,19]. It does not involve limitations similar to those characteristic of the CWA, and it provides a better convergence. The disadvantages of this method include its being mathematically complicated, as well as numerous “peculiarities” involved in numerical realization. Besides, application of the IM to cases of heterogeneous or anisotropic media meets with difficulties; however, with the volume integral method it is possible to overcome these difficulties. Nevertheless, it is on the basis of this theory that all the well-known problems of diffraction by periodic and nonperiodic structures in optics and other fields have been solved. In many cases it offers the only possible way to follow up in research [3,20,21]. The flexibility and universality inherent in the IM, in particular, enable one to reduce rather easily the problem of radiation of Gaussian waves or of a localized source to that of plane-wave incidence, for which scientists all over the world have a set of numerical solutions. Generalizations of the IM have recently been proposed for arbitrarily profiled 1D multilayer gratings [22], randomly rough x-ray-extreme-UV mirrors [23], conical diffraction gratings including materials with a negative permittivity and permeability [19,24,25], arbitrarily rough multilayer 1D gratings and mirrors [26], biperiodic anisotropic structures using a variation formulation [27], Fresnel zone plates and diffraction optical elements [28,29], and 3D PBGs of some geometries using volume [7] and surface [30] integrals, among others.

The motivation for the present work is to introduce the new method as an exact and universal approach to be applied in areas where rapid design and analysis of the most sensitive PBG cases would be at a premium. The corresponding theory is described in Sec. II. The diffraction problem and boundary relations between values of the fields across the boundary are formulated in Sec. II A. The method of scattering amplitude matrices (S -matrix algorithm) expedient for the calculation of far fields and polarization properties of conical diffraction by PBGs is described in Sec. II B. The respective integral equations in terms of boundary potentials are given in Sec. II C. Numerical implementation of the developed theory is described briefly in Sec. III. Diverse numerical tests devoted to applying the method and obtaining results for sensitive cases of various PBGs are given in Sec. IV. In Sec. IV A we compare our results with data obtained with the other well-established approach and give examples of the significant impact of rod shape and filling ratio on diffraction in metallic PBGs supporting polariton-plasmon excitation, particularly, close to resonances. In Sec. IV B we demonstrate the influence of high conductivity on transmission spectra of lossless PBGs supporting waveguide modes in different polarization states.

In Sec. IV C we calculate transmission spectra of dielectric PBGs supporting Bragg resonances in conical diffraction.

II. THEORY

We employed the IM for a theoretical description of the optical properties of PBGs. The theory of diffraction on separated boundaries is covered here necessarily on the whole because its main parts including mathematical aspects have been derived at considerable length in Refs. [19,25,26,31,32]. The electromagnetic formulation of diffraction by gratings, which are modeled as infinite periodic structures, can be reduced to a system of Helmholtz equations for the z components of the electric and magnetic fields in \mathbb{R}^2 , where the solutions have to be quasiperiodic in the x direction, to be subject to radiation conditions in the y direction, and to satisfy certain jump conditions at the interfaces between different materials of the diffraction grating. In the case of classical diffraction, when \mathbf{k} is orthogonal to the z direction, the system splits into independent problems for the two basic polarizations of the incident wave, whereas in the case of conical diffraction (Fig. 1) the boundary values of the field z components, as well as their normal and tangential derivatives at the interfaces, are coupled. Thus the unknowns are scalar functions in the case of classical diffraction and two-component vector functions in the conical case. A grating diffracts the incoming plane wave into a finite number of outgoing plane waves, the so-called reflected and transmitted modes or orders. The program computes the energies and polarizations of these modes for an arbitrary number of layers with different boundary profile types including closed boundary profiles (i.e., inclusions). The boundary profiles of the layers must be strictly separated, i.e., the maximal y value of a given profile is strictly less than the minimal y value of the next profile above. In this case, it is possible to determine the diffracted field of the grating by computing scattering amplitude matrices separately for any profile. For each interface between two different materials, the computation of the scattering amplitude matrices corresponds to solving one-boundary conical diffraction problems with plane waves illuminating the interface from above and below. Using the integral method one has to solve for each interface a 2×2 system of singular integral equations with different right-hand sides. The equations are discretized with a collocation method, the unknowns are sought as trigonometric

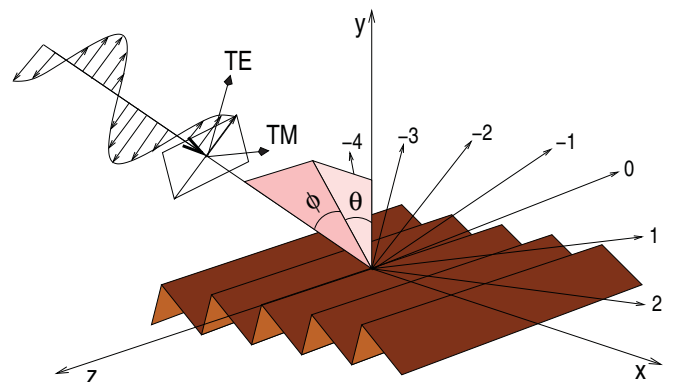


FIG. 1. (Color online) Schematic conical diffraction by a grating.

polynomials, which, in the case of profiles with edges, are partially replaced by splines to improve the approximation of the solution near the edges.

A. Diffraction problem

In the multiboundary diffraction problem one has to deal with cylindrical surfaces $\Sigma_n \times \mathbb{R}$, $n = 0, \dots, N-1$, either open or closed, which are d periodic in x and whose generatrices are parallel to the z axis (Fig. 2). The surfaces separate $N+1$ periodic regions $G_n \times \mathbb{R}$, filled with material of constant permittivity and permeability. The grating structure is characterized by piecewise constant functions of electric permittivity ε and magnetic permeability μ , which are d periodic in x , homogeneous in z , and have jumps at the surfaces Σ_n . The values of these functions in the semi-infinite regions $G_0 \times \mathbb{R}$ above and $G_N \times \mathbb{R}$ below the inhomogeneous structure are denoted ε_0, μ_0 and ε_N, μ_N , respectively. We assume that $\lambda = 2\pi c/\omega$ with a light velocity c at a given pulsance ω , and the incident time-harmonic field with polarization vectors \mathbf{p} and \mathbf{s} , defined later, is given by

$$(\mathbf{E}^i, \mathbf{H}^i) = (\mathbf{p}, \mathbf{s}) e^{-i\omega t} e^{i(\alpha x - \beta y + \gamma z)},$$

where $(\alpha, -\beta, \gamma) = \omega \sqrt{\varepsilon_0 \mu_0} (\sin \theta \cos \phi, -\cos \theta \cos \phi, \sin \phi)$, and $|\theta|, |\phi| < \pi/2$.

Due to the periodicity of the surfaces the incident wave is scattered into a finite number of plane waves in $G_0 \times \mathbb{R}$ and also in $G_N \times \mathbb{R}$ if $\varepsilon_N \mu_N > 0$. The wave vectors of these outgoing orders lie on the surface of a cone whose axis is parallel to the z axis. Therefore one speaks of conical diffraction. Classical diffraction corresponds to $\gamma = 0$, whereas $\gamma \neq 0$ characterizes conical diffraction. Using the representation of the total field $\mathbf{E}(x, y, z) = E(x, y) e^{i\gamma z}$, $\mathbf{H}(x, y, z) = \sqrt{\varepsilon_0/\mu_0} B(x, y) e^{i\gamma z}$, the system of time-harmonic Maxwell equations transforms to 2D Helmholtz equations in the domains G_n , where ε and μ are constant,

$$[\Delta + (\omega\kappa)^2]E(x, y) = [\Delta + (\omega\kappa)^2]B(x, y) = 0, \quad (1)$$

with the coefficient function $(\omega\kappa)^2 = \omega^2 \varepsilon \mu - \gamma^2$ piecewise constant and d periodic in x .

It can be shown that under the condition $\kappa \neq 0$, which is assumed throughout, the z components E_z and B_z of the vector functions E and B determine the total electromagnetic field

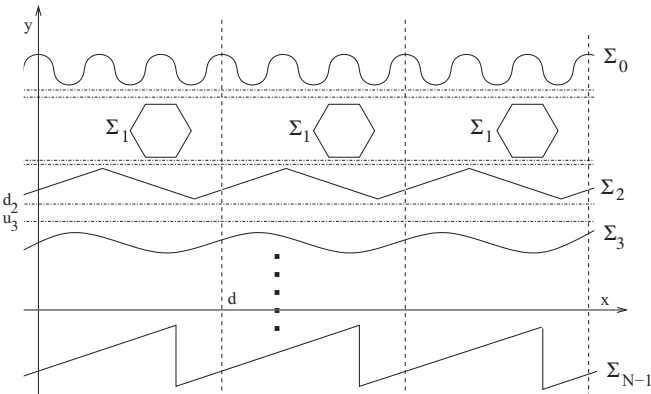


FIG. 2. Cross section of a grating with separated boundaries.

(\mathbf{E}, \mathbf{H}) . The continuity of the tangential components of \mathbf{E} and \mathbf{H} on the surface Σ_n implies jump conditions for E_z, B_z in the form (see Ref. [19])

$$\begin{aligned} [E_z]_{\Sigma_n} &= [H_z]_{\Sigma_n} = 0, \\ \left[\frac{\varepsilon \partial_\nu E_z}{\kappa^2} \right]_{\Sigma_n} &= -\varepsilon_0 \sin \phi \left[\frac{\partial_t B_z}{\kappa^2} \right]_{\Sigma_n}, \\ \left[\frac{\mu \partial_\nu B_z}{\kappa^2} \right]_{\Sigma_n} &= \mu_0 \sin \phi \left[\frac{\partial_t E_z}{\kappa^2} \right]_{\Sigma_n}, \end{aligned} \quad (2)$$

where $[\cdot]$ denotes the jump of functions on Σ_n , and $\partial_\nu = \nu_x \partial_x + \nu_y \partial_y$ and $\partial_t = -\nu_y \partial_x + \nu_x \partial_y$ are the normal and tangential derivatives on Σ_n , respectively. The z components of the incoming field,

$$\begin{aligned} E_z^i(x, y) &= p_z e^{i(\alpha x - \beta y)}, \\ B_z^i(x, y) &= s_z e^{i(\alpha x - \beta y)} \sqrt{\mu_0/\varepsilon_0} = q_z e^{i(\alpha x - \beta y)}, \end{aligned}$$

are α quasiperiodic in x of period d . Here the vector \mathbf{s} is orthogonal to the plane spanned by \mathbf{k} and the grating normal $\mathbf{v} = (0, 1, 0)$ and \mathbf{p} lies in that plane:

$$\mathbf{s} = \mathbf{k} \times (0, 1, 0) / |\mathbf{k} \times (0, 1, 0)|, \quad \mathbf{p} = \mathbf{s} \times \mathbf{k} / |\mathbf{k}|.$$

If $\mathbf{k} = (0, -k, 0)$, we set $\mathbf{s} = (0, 0, 1)$ and hence $\mathbf{p} = (1, 0, 0)$. Then, the incident plane wave is given by its polarization angles

$$\delta = \arctan[|(\mathbf{E}^i, \mathbf{s})|/|(\mathbf{E}^i, \mathbf{p})|], \quad \psi = -\arg[(\mathbf{E}^i, \mathbf{s})/(\mathbf{E}^i, \mathbf{p})],$$

where $\delta \in [0, \pi/2]$, $\psi \in (-\pi, \pi]$. Since \mathbf{E}^i is orthogonal to the wave vector, $(\mathbf{E}^i, \mathbf{k}) = 0$, one can decompose \mathbf{E}^i :

$$\mathbf{E}^i = (\mathbf{E}^i, \mathbf{s}) \mathbf{s} + (\mathbf{E}^i, \mathbf{p}) \mathbf{p}.$$

It is easy to see that for incident and also diffracted field components (\mathbf{E}, \mathbf{q}) and (\mathbf{E}, \mathbf{p}) with propagation angles θ and ϕ and $\rho = \cos \phi (\sin^2 \theta \cos^2 \phi + \sin^2 \phi)^{0.5}$,

$$(\mathbf{E}, \mathbf{q}) = (E_z \sin \theta - B_z \cos \theta \sin \phi) / \rho,$$

$$(\mathbf{E}, \mathbf{p}) = (E_z \cos \theta \sin \phi + B_z \sin \theta) / \rho,$$

where, if $\mathbf{k} \parallel \mathbf{v}$, then $(\mathbf{E}^i, \mathbf{q}) = E_z^i$ and $(\mathbf{E}^i, \mathbf{p}) = B_z^i$. The incident values (E_z^i, B_z^i) can be defined from these equations for the given incidence (θ, ϕ) and polarization (δ, ψ) angles under some normalization condition [31].

We seek a bounded H^1 -regular solution (E_z, B_z) which is α quasiperiodic in x [$u(x+d, y) = e^{i\alpha d} u(x, y)$] and satisfies the radiation conditions

$$\begin{aligned} (E_z, B_z) &= (E_z^i, B_z^i) + \sum_{m \in \mathbb{Z}} (E_0^m, B_0^m) e^{i(\alpha_m x + \beta_0^m y)} \\ &\text{for } y \geq \sup \Sigma_0, \\ (E_z, B_z) &= \sum_{m \in \mathbb{Z}} (E_N^m, B_N^m) e^{i(\alpha_m x - \beta_N^m y)} \\ &\text{for } y \leq \inf \Sigma_{N-1}, \end{aligned} \quad (3)$$

where $\alpha_m = \alpha + 2\pi m/d$ and $\beta_n^m = \sqrt{\omega^2 \varepsilon_n \mu_n - \gamma^2 - \alpha_m^2}$ with $0 \leq \arg \beta_n^m < \pi$. In the following it is always assumed that, besides $\varepsilon_0, \mu_0 > 0$,

$$0 \leq \arg \varepsilon, \quad \arg \mu \leq \pi, \quad \arg(\varepsilon \mu) < 2\pi,$$

which holds for all existing optical (meta)materials [25]. Then the electromagnetic formulation of conical diffraction on multiboundary gratings is equivalent to Eqs. (1)–(3) for (E_z, B_z) .

B. S-matrix approach

Since the grating profiles are strictly separated, the problem, Eqs. (1)–(3), can be treated using certain robust algorithms for modeling layered gratings (an overview is given, e.g., in Ref. [33]). The present method extends the S-matrix algorithm given in Ref. [34] for the integral method and the in-plane case. As we know, the first description of the scattering amplitude matrices algorithm has been done in Ref. [35]. Its application to the off-plane case is described in Refs. [29,32]. Here we give an exact description of the S-matrix algorithm combined effectively with the conical integral equations formulated for solving such multilayer grating problems.

Between surface Σ_{n-1} and surface Σ_n for all $n = 1, \dots, N$, there exist strips $\{u_n < y < d_{n-1}\}$ which do not cross the interfaces for $n = 1, \dots, N$ (Fig. 2). In any strip $\{u_n < y < d_{n-1}\}$ with the cut wave number κ_n , the solution (E_z, B_z) has the series expansion

$$(E_z, B_z) = \sum_{m \in \mathbb{Z}} ((a_n^m, c_n^m) e^{i\beta_n^m y} + (b_n^m, d_n^m) e^{-i\beta_n^m y}) e^{i\alpha_m x}.$$

Let $y_n \in (u_n, d_{n-1})$ and denote

$$\begin{aligned} (A_n^m, C_n^m) &= e^{-i\beta_n^m y_n} (a_n^m, c_n^m), \\ (\mathcal{A}_n^m, \mathcal{C}_n^m) &= e^{-i\beta_{n+1}^m y_n} (a_{n+1}^m, c_{n+1}^m), \\ (B_n^m, D_n^m) &= e^{-i\beta_n^m y_n} (b_n^m, d_n^m), \\ (\mathcal{B}_n^m, \mathcal{D}_n^m) &= e^{-i\beta_{n+1}^m y_n} (b_{n+1}^m, d_{n+1}^m). \end{aligned}$$

Then in the strip $\{u_n < y < d_{n-1}\}$ above Σ_n ,

$$(E_z, B_z) = \sum_{m \in \mathbb{Z}} ((A_n^m, C_n^m) e^{i\beta_n^m (y-y_n)} + (B_n^m, D_n^m) e^{-i\beta_n^m (y-y_n)}) e^{i\alpha_m x},$$

and in the strip $\{u_{n+1} < y < d_n\}$ below Σ_n ,

$$(E_z, B_z) = \sum_{m \in \mathbb{Z}} ((\mathcal{A}_n^m, \mathcal{C}_n^m) e^{i\beta_{n+1}^m (y-y_n)} + (\mathcal{B}_n^m, \mathcal{D}_n^m) e^{-i\beta_{n+1}^m (y-y_n)}) e^{i\alpha_m x},$$

with amplitudes of incoming A_n, B_n and diffracted B_n, \mathcal{A}_n waves defined as

$$\begin{aligned} A_n &= \{(A_n^m, C_n^m)\}_{m \in \mathbb{Z}}, & B_n &= \{(B_n^m, D_n^m)\}_{m \in \mathbb{Z}}, \\ B_n &= \{(\mathcal{B}_n^m, \mathcal{D}_n^m)\}_{m \in \mathbb{Z}}, & \mathcal{A}_n &= \{(\mathcal{A}_n^m, \mathcal{C}_n^m)\}_{m \in \mathbb{Z}}. \end{aligned}$$

The multiprofile problem, Eqs. (1)–(3), is solved if the scattering amplitude columns B_0 and \mathcal{A}_{N-1} are expressed for a given input A_0 and vanishing \mathcal{B}_{N-1} . The S-matrix method looks for a recursion of operators R_j, T_j such that

$$B_n = R_n A_n, \quad \mathcal{A}_{N-1} = T_n A_n, \quad n = N-1, \dots, 0.$$

The scattering amplitude columns are connected by two types of relations,

$$\begin{aligned} A_{n-1} &= \gamma_n^{-1} A_n, & B_{n-1} &= \gamma_n B_n, \\ \gamma_n &= \text{diag} \{ \exp(i\beta_n^m (y_{n-1} - y_n)) \}_{m \in \mathbb{Z}}, \\ B_n &= r_n A_n + t'_n \mathcal{B}_n, & \mathcal{A}_n &= t'_n A_n + r'_n \mathcal{B}_n, \end{aligned}$$

where r_n or r'_n and t_n or t'_n are reflection and transmission operators, respectively, for the illumination of Σ_n from above or below. This leads to a simple recursion starting from below,

$$\begin{aligned} R_{n-1} &= r_{n-1} + t'_{n-1} \gamma_n R_n (I - \gamma_n r'_{n-1} \gamma_n R_n)^{-1} \gamma_n t_{n-1}, \\ T_{n-1} &= T_n (I - \gamma_n r'_{n-1} \gamma_n R_n)^{-1} \gamma_n t_{n-1}, \end{aligned} \quad (4)$$

with the unity operator I and initial values

$$R_{N-1} = r_{N-1}, \quad T_{N-1} = t_{N-1}.$$

Finally, one gets the desired amplitude vectors:

$$B_0 = R_0 A_0, \quad \mathcal{A}_{N-1} = T_0 A_0. \quad (5)$$

It is worth noting that recursion (4) is stable, since the elements of γ_n have norms ≤ 1 and can be used for any number of closed and continuous boundaries having any conductivity.

C. Integral equations

The reflection and transmission operators r_n, r'_n, t_n , and t'_n of a given profile Σ_n , which separates two domains, are obtained from the response of that one-profile grating illuminated by plane waves from above and below. For definiteness we label the domains G_n and G_{n+1} and the corresponding material coefficients ε_n, μ_n and $\varepsilon_{n+1}, \mu_{n+1}$. If the surface Σ_n is continuous, then G_{n+1} denotes the domain below Σ_n , whereas for closed boundary profiles the domain G_{n+1} denotes one of the inclusions inside Σ_n . For off-plane diffraction one has to find the Rayleigh coefficients of the diffracted fields for input waves with z components,

$$\begin{pmatrix} E_\delta^+ \\ B_\delta^+ \end{pmatrix} = \begin{pmatrix} 1 - \delta \\ \delta \end{pmatrix} e^{i(\alpha_m x - \beta_n^m y)}, \quad \delta = 0, 1,$$

incident from above and

$$\begin{aligned} \begin{pmatrix} E_\delta^- \\ B_\delta^- \end{pmatrix} &= \begin{pmatrix} 1 - \delta \\ \delta \end{pmatrix} e^{i(\alpha_m x + \beta_{n+1}^m y)} \\ \text{or} \quad \begin{pmatrix} E_\delta^- \\ B_\delta^- \end{pmatrix} &= \begin{pmatrix} 1 - \delta \\ \delta \end{pmatrix} e^{i(\alpha_m x + \beta_n^m y)}, \quad \delta = 0, 1, \end{aligned}$$

incident from below for continuous Σ_n or inclusions, respectively.

For illumination from above, one has to solve the following problem: Setting

$$E_z = \begin{cases} u_n + E_\delta^+, & B_z = \begin{cases} v_n + B_\delta^+ & \text{in } G_n, \\ v_{n+1} & \text{in } G_{n+1}, \end{cases} \\ u_{n+1}, & \end{cases}$$

find α -quasiperiodic solutions of the Helmholtz equations

$$(\Delta + (\omega \kappa_n)^2) u_n = (\Delta + (\omega \kappa_n)^2) v_n = 0, \quad (6)$$

$$(\Delta + (\omega \kappa_{n+1})^2) u_{n+1} = (\Delta + (\omega \kappa_{n+1})^2) v_{n+1} = 0, \quad (7)$$

where now $\kappa_n^2 = \varepsilon_n \mu_n - \varepsilon_0 \mu_0 \sin^2 \phi$. From Eq. (2) one gets the jump conditions on Σ_n :

$$\begin{aligned} u_{n+1} &= u_n + E_\delta^+, \quad v_{n+1} = v_n + B_\delta^+, \\ \frac{\varepsilon_{n+1} \partial_\nu u_{n+1}}{\kappa_{n+1}^2} - \frac{\varepsilon_n \partial_\nu (u_n + E_\delta^+)}{\kappa_n^2} &= \frac{\varepsilon_0 \sin \phi (\kappa_{n+1}^2 - \kappa_n^2)}{\kappa_n^2 \kappa_{n+1}^2} \partial_t v_{n+1}, \\ \frac{\mu_{n+1} \partial_\nu v_{n+1}}{\kappa_{n+1}^2} - \frac{\mu_n \partial_\nu (v_n + B_\delta^+)}{\kappa_n^2} &= -\frac{\mu_0 \sin \phi (\kappa_{n+1}^2 - \kappa_n^2)}{\kappa_n^2 \kappa_{n+1}^2} \partial_t u_{n+1}. \end{aligned}$$

For illumination from below we set

$$E_z = \begin{cases} u_n, & \text{in } G_n, \\ u_{n+1} + E_\delta^-, & \text{in } G_{n+1}. \end{cases} \quad B_z = \begin{cases} v_n & \text{in } G_n, \\ v_{n+1} + B_\delta^- & \text{in } G_{n+1}. \end{cases}$$

The α -quasiperiodic functions u_j, v_j have to satisfy the Helmholtz equations, (6) and (7), and the transmission conditions

$$\begin{aligned} u_{n+1} + E_\delta^- &= u_n, \quad v_{n+1} + B_\delta^- = v_n, \\ \frac{\varepsilon_{n+1} \partial_\nu (u_{n+1} + E_\delta^-)}{\kappa_{n+1}^2} - \frac{\varepsilon_n \partial_\nu u_n}{\kappa_n^2} &= \frac{\varepsilon_0 \sin \phi (\kappa_{n+1}^2 - \kappa_n^2)}{\kappa_n^2 \kappa_{n+1}^2} \partial_t v_n, \\ \frac{\mu_{n+1} \partial_\nu (v_{n+1} + B_\delta^-)}{\kappa_{n+1}^2} - \frac{\mu_n \partial_\nu v_n}{\kappa_n^2} &= -\frac{\mu_0 \sin \phi (\kappa_{n+1}^2 - \kappa_n^2)}{\kappa_n^2 \kappa_{n+1}^2} \partial_t u_n. \end{aligned}$$

The solution of these general one-boundary conical diffraction problems is derived by using a combination of the direct (Green's formula) and indirect (via layer potentials) boundary integral approaches. In G_{n+1} the functions u_{n+1}, v_{n+1} are represented as single-layer potentials with densities w, τ on Γ_n , denoting one period of Σ_n ,

$$\begin{aligned} u_{n+1}(P) &= \int_{\Gamma_n} w(Q) \Psi_{\kappa_{n+1}}(P - Q) d\sigma_Q, \\ v_{n+1}(P) &= \int_{\Gamma_n} \tau(Q) \Psi_{\kappa_{n+1}}(P - Q) d\sigma_Q, \end{aligned}$$

where $P = (X, Y)$ and $d\sigma_Q$ denotes the integration with respect to the arc length. The integral kernel $\Psi_{\kappa_{n+1}}$ is the α -quasiperiodic fundamental solution of period d , with logarithmic singularities at points $\{(md, 0)\}$ given by the infinite series

$$\Psi_{\kappa_{n+1}}(P) = \frac{i}{4} \sum_{m=-\infty}^{\infty} H_0^{(1)}(\omega \kappa_{n+1} \sqrt{(X - md)^2 + Y^2}) e^{im d \alpha},$$

where $H_0^{(1)}$ is the first Hankel function of zero order. Based on the known jump relations for layer potentials, one concludes, as in Ref. [19], that the transmission conditions on Σ_n are fulfilled only if the functions w, τ are solutions of the system

of integral equations,

$$\begin{aligned} \frac{\varepsilon_{n+1} \kappa_n^2}{\varepsilon_n \kappa_{n+1}^2} V_n (L_{n+1} - I) w - (I + K_n) V_{n+1} w &+ \varepsilon_0 \sin \phi \left(1 - \frac{\kappa_n^2}{\kappa_{n+1}^2}\right) H_n V_{n+1} \tau = \mathcal{U}, \\ \frac{\mu_{n+1} \kappa_n^2}{\mu_n \kappa_{n+1}^2} V_n (L_{n+1} - I) \tau - (I + K_n) V_{n+1} \tau &- \mu_0 \sin \phi \left(1 - \frac{\kappa_n^2}{\kappa_{n+1}^2}\right) H_n V_{n+1} w = \mathcal{V}, \end{aligned} \quad (8)$$

$P \in \Sigma_n$, with right-hand sides \mathcal{U} and \mathcal{V} determined by the input waves E_δ^\pm and B_δ^\pm . Here the integral operators V_n and K_n are the single- and double-layer potentials

$$\begin{aligned} V_n \varphi(P) &= 2 \int_{\Gamma_n} \varphi(Q) \Psi_{\kappa_n}(P - Q) d\sigma_Q, \quad P \in \Sigma_n, \\ K_n \varphi(P) &= 2 \int_{\Gamma_n} \varphi(Q) \partial_{\nu(Q)} \Psi_{\kappa_n}(P - Q) d\sigma_Q, \end{aligned}$$

where $\nu(Q)$ is the normal to Σ_n at Q pointing into G_{n+1} . These boundary integral operators as well as the adjoint of the double-layer potential,

$$L_n \varphi(P) = 2 \int_{\Gamma_n} \varphi(Q) \partial_{\nu(P)} \Psi_{\kappa_n}(P - Q) d\sigma_Q,$$

appear already in integral methods for classical diffraction. The presence of tangential derivatives in the jump conditions for solutions of conical diffraction leads to a new boundary integral:

$$H_n \varphi(P) = 2 \int_{\Gamma_n} \varphi(Q) \partial_{t(Q)} \Psi_{\kappa_n}(P - Q) d\sigma_Q.$$

Since the kernel of this integral operator is strongly singular, $H_n \varphi$ has to be interpreted as a principal value integral, and therefore Eq. (8) represent a system of singular integral equations.

Properties of this system are described in Refs. [19,25] for the case of incident plane waves from above, where one gets

$$\mathcal{U} = -2E_\delta^+, \quad \mathcal{V} = -2B_\delta^+$$

as the right-hand sides of Eq. (8). Analogously, for illumination from below the transmission conditions on Σ_n lead to the right-hand sides

$$\begin{aligned} \mathcal{U} &= \frac{\varepsilon_{n+1} \kappa_n^2}{\varepsilon_n \kappa_{n+1}^2} V_n \partial_\nu E_\delta^- - (I + K_n) E_\delta^- \\ &+ \varepsilon_0 \sin \phi \left(1 - \frac{\kappa_n^2}{\kappa_{n+1}^2}\right) H_n B_\delta^-, \\ \mathcal{V} &= \frac{\mu_{n+1} \kappa_n^2}{\mu_n \kappa_{n+1}^2} V_n \partial_\nu B_\delta^- - (I + K_n) B_\delta^- \\ &- \mu_0 \sin \phi \left(1 - \frac{\kappa_n^2}{\kappa_{n+1}^2}\right) H_n E_\delta^- \end{aligned}$$

in the case of a continuous profile and

$$\mathcal{U} = -2E_\delta^-, \quad \mathcal{V} = -2B_\delta^-$$

for closed boundary profiles.

The advantage of our integral formulation, Eqs. (4)–(8), is a clever combination of the integral equations with the S -matrix algorithm allowing one to solve the single discrete problem for computing scattering amplitude matrices of Eq. (4). As a result, the computation of the discrete matrix on the left of Eq. (8) and its factorization have to be performed only once for that profile due to the unified treatment of different incoming waves.

III. NUMERICAL IMPLEMENTATION

We discuss briefly the numerical solution of systems (4)–(8). In the computations the indices $m \in [M_0, M_1]$ are chosen such that at least all propagating modes for all one-profile gratings are covered; i.e., we require that $\beta_n^m \notin \mathbb{R}$ for all $m \notin [M_0, M_1]$ and n . Thus, by solving Eq. (8) for $M = 2(M_1 - M_0 + 1)$ incident waves E_δ^+, B_δ^+ and computing the scattering amplitudes for all modes $m \in [M_0, M_1]$ of u_n, v_n and u_{n+1}, v_{n+1} , we derive $M \times M$ reflection and transmission matrices r_n and t_n for illumination from above. Analogously, the $M \times M$ reflection and transmission matrices r'_n and t'_n are obtained from Eq. (8) with M incident waves E_δ^-, B_δ^- , illuminating the profile from the below. These reflection and transmission matrices for each boundary profile are computed simultaneously as described above.

The kernels of the integrals V_n have a logarithmic singularity like $\log|s - t|$ and H_n is a singular integral operator with the kernel singularity $1/(s - t)$ as $t \rightarrow s$. Therefore the discretization of the integrals requires some caution, especially if the profile has corners, where additionally the kernels of K_n and L_n have fixed singularities. The integral equations are discretized with a collocation method, and the unknowns are sought as trigonometric polynomials, which, in the case of gratings with edges, are partially replaced by splines to improve the approximation of the solution near the profile corners [19]. The trigonometric collocation method with special treatment of singular integrals gives, for smooth boundary profiles with the number of collocation points \mathcal{N} , a convergence rate of order $O(\mathcal{N}^{-3})$. The hybrid trigonometric-spline collocation with mesh grading near corners gives a convergence rate of order $O(\mathcal{N}^{-2})$.

Expressions (4) allow us to find amplitude matrices by a recursive procedure beginning with the lower medium. To do this, we have to know, in the general case, four matrices of scattering amplitudes and perform two matrix inversions in each iteration step. The computation time for one-boundary problems was shown to scale quadratically with the main accuracy parameter (the number of collocation points) [19]. The computation time is also linearly proportional to the number of boundaries. Using Hankel functions as fundamental solutions for closed boundaries decreases the number of required collocation points in several times. The memory cache for amplitude matrices of multilayer grating problems (e.g., photonic crystals) with the same boundary profiles and the same pairs or quads of layers can be used.

The code developed and tested is found to be accurate and efficient for solving various in-plane and off-plane diffraction problems, including high-conductive gratings, surfaces with edges, real groove profiles, and gratings with nonfunction boundary profiles. Extension to rod gratings and 2D PBGs

is naturally obtained. The high rate of convergence, the high accuracy, and the short computation time of the suggested solver are further demonstrated for various nontrivial numerical examples.

IV. COMPUTATION OF PBG EXAMPLES IN SENSITIVE CASES

The workability of the code developed has been confirmed by numerous tests usually employed in classical and conical diffraction cases: more specifically, the reciprocity theorem; stabilization of results under doubling of the number of collocation points and variation of the calculation accuracy of kernel functions; comparison with analytically amenable cases of plane interfaces; consideration of the inverse (nonphysical) radiation condition; use of different variants of the collocation point distribution on boundaries (mesh refinements); and comparison with the results obtained by another of our codes or with published data, or with information submitted to us by other researchers, including results of measurements. A small portion of such numerical tests devoted to the analysis of sensitive cases of various PBGs is demonstrated in this section. The presented results demonstrate the impact of rod shape on diffraction in PBGs supporting polariton-plasmon excitation and other types of anomalies (i.e., waveguiding anomalies, cavity modes, Fabry-Perot resonances, Rayleigh orders, etc.), particularly in the vicinity of resonances and at high filling ratios. In conical diffraction, the influence of all possible types of waves can be mixed.

A. PBGs with nanorods supporting polariton-plasmon excitation

In this section, we analyze numerically the optical response of photonic crystal slabs supporting polariton-plasmon excitation with different cross sections of nanowires invariant with respect to the z axis and different numbers of gratings stacked one upon the other. The essential physics of the formation of individually localized plasmon polariton modes (so-called particle plasmons) in multilayer metallic nanowire arrays is well described in Ref. [36]. As far as we know from the literature, there is no detailed description of the influence of very different rod geometries and of the filling factor on PBGs with nanowires supporting polariton-plasmon excitation. The model contains $N - 1$ identical gratings of arbitrary cross section displaced vertically (by H_n) and horizontally (by L_n) relative to one another and embedded in a homogeneous medium with dielectric permittivity ϵ_1 and magnetic susceptibility μ_1 . We deal here only with materials with $\mu_n = 1$, although the model is applicable to other cases as well, including metamaterials [19]. The dependence of the dielectric permittivity ϵ_2 of the material of nanorods on the incident photon frequency is assumed to be known. The lower medium (substrate) and the upper one are likewise assigned pairs of material constants, but one may conceive of more complicated cases of multilayer structures as well. The model also allows an arbitrary incidence of, in the general case, elliptically polarized radiation on PBGs, which is prescribed by two angles of incidence and two angles of polarization.

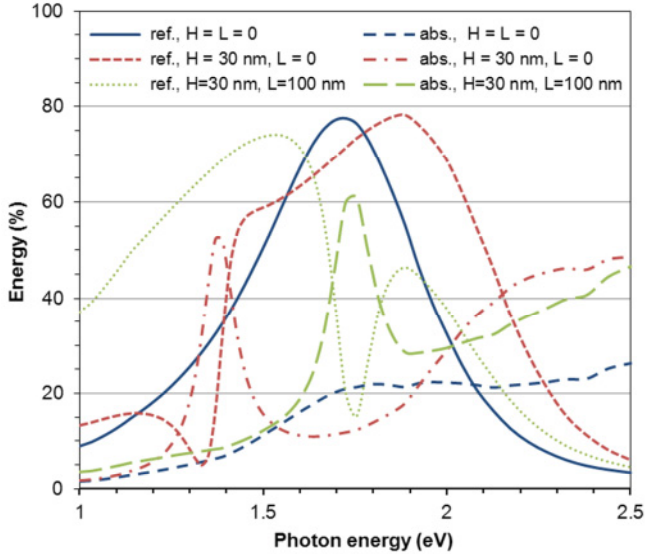


FIG. 3. (Color online) Calculated reflection and absorption spectra of SiO₂-embedded $d = 200$ nm gratings with Au nanowires of 100×15 nm² rectangular cross section and different vertical, H , and horizontal, L , displacements are plotted vs photon energy for normal incidence and TM polarization.

In Fig. 3, calculated spectra of reflected energy for PBGs with Au nanowires of rectangular cross section, measuring 100×15 nm² and $N - 1 = 1$ ($H = L = 0$) or $N - 1 = 2$ ($H = 30$ nm, $L = 0$ and $H = 30$ nm, $L = 100$ nm), are compared with similar spectra derived in Fig. 3(a) in Ref. [36] by the plane-wave expansion approach. We consider here TM-polarized radiation (the plane of polarization is perpendicular to the lines) incident normally with respect to the x - z plane) on a grating with a period $d = 200$ nm and refractive indices of Au taken from Ref. [37]. To eliminate interference effects, the Au nanorods are embedded in an infinite homogeneous fused silica matrix with dielectric permittivity $\epsilon_{0,1,3} = 2.13$. Examining the two figures, we see a very good agreement, which supports the applicability of both rigorous numerical methods to the analysis of diffraction on such PBGs with rectangular slabs.

Figure 4 displays, for comparison, theoretical spectra of energy reflected from, and absorbed by, a PBG with Au nanowires of circular, square, rectangular, and triangular cross sections of the same area and with $N - 1 = 1$ studied in the range 1–3 eV (visible and near-infrared). In this and subsequent examples we consider TM-polarized light normally falling on Au nanowires embedded in a SiO₂ matrix with $d = 200$ nm and refractive indices of Au taken from Ref. [38]. The orientation of the rods having edges is chosen in such a way that light normally falls on one side of the rods only. The $a \times b$ dimensions of the rectangular rods selected for this example are 50×25 or 25×50 nm² and the width of the squares or triangles and diameter of the circles were chosen to obtain equal cross-sectional areas $S = 1250$ nm². As shown in Fig. 4, reflection and, particularly, absorption spectra exhibit a strong difference near the plasmon-polariton anomaly among the five shapes of nanowire cross sections chosen. These differences amount to several hundred percent for the rectangles because of their different width-to-height

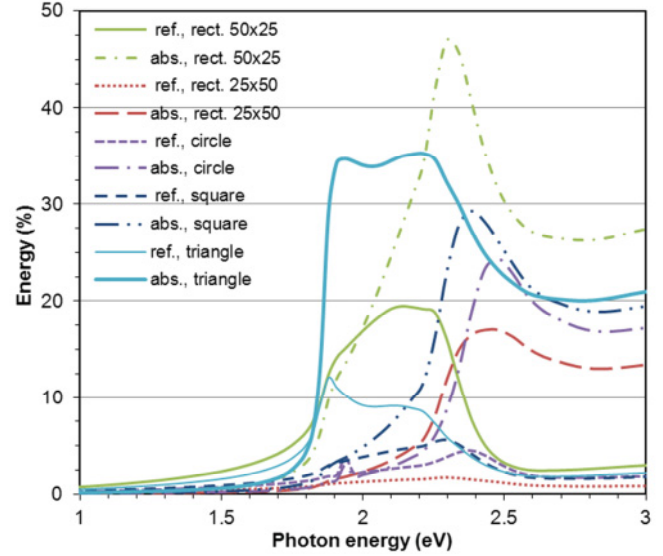


FIG. 4. (Color online) Calculated reflection and absorption spectra of SiO₂-embedded $d = 200$ nm gratings with Au nanowires of different cross sections, the same area of $S = 1250$ nm², and $H = L = 0$ ($N - 1 = 1$) are plotted vs photon energy for normal incidence and TM polarization.

ratio (2 and 0.5) compared with the square or the circle (1) and the equilateral triangle (0.866). One also observes a noticeable difference in the positions of the absorption and reflection maxima among different grating profiles. Thus, the simple effective medium theory cannot be applied to the design and analysis of such PBGs, even for a low filling ratio.

Figure 5 presents energy spectra similar to those displayed in Fig. 4 but for S four times that in the preceding example. In this case, $a \times b = 100 \times 50$ nm² or 50×100 nm². We readily see that the differences in the reflection and absorption spectra among gratings of different profiles increase with increasing filling ratio and are observed now not just close to the plasmon resonances. Near the resonances, they amount to a few tens

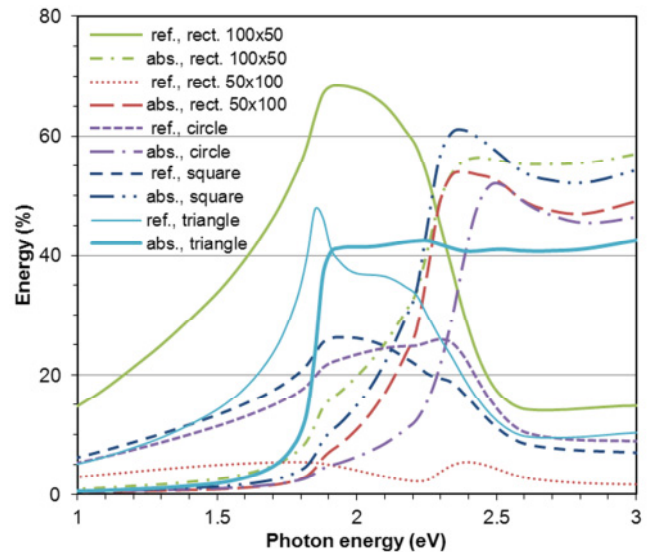


FIG. 5. (Color online) The same as Fig. 4, but for the same nanowire cross section area of $S = 5000$ nm².

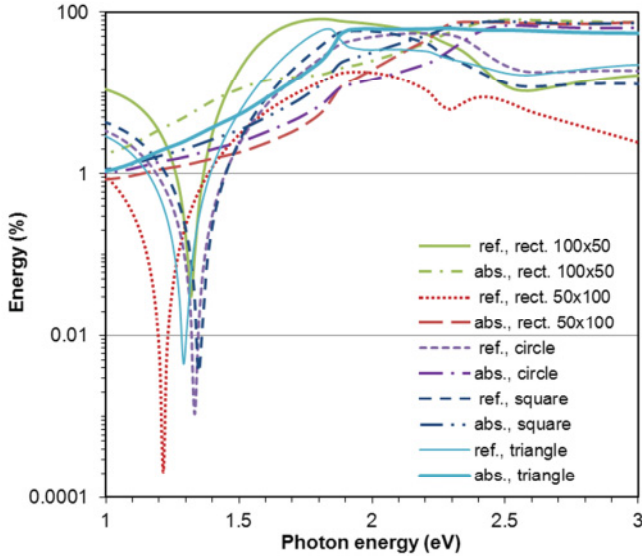


FIG. 6. (Color online) Calculated reflection and absorption spectra of SiO_2 -embedded $d = 200$ nm gratings with Au nanowires of different cross sections, the same area $S = 5000$ nm^2 , and $N - 1 = 2$, $H = 50$ nm, $L = 0$ are plotted vs photon energy for normal incidence and TM polarization.

percent of energy (Fig. 5). Absorption spectra of triangular-shaped nanowires have an interesting band-gap-like structure that is not the case for absorption spectra of nanowires of other rod shapes.

Figure 6 shows spectra similar to those depicted in Fig. 5 but for $N - 1 = 2$, $H = 50$ nm, and $L = 0$. In the case of two gratings, the plasmon-polariton resonance frequencies are subtracted or summed [36], and one may expect still larger differences in the spectra of reflected and absorbed energy among crystals with lattice cells of different shapes. Indeed, Fig. 6 drawn on a log scale reveals enormous differences, up to orders of magnitude, throughout the spectrum studied. The minimum reflectance of $\sim 10^{-6}$ is observed for a PBG with a rectangular cross section of 100×50 nm^2 . The positions of the reflection minima are also very different for different rod shapes.

Only $\mathcal{N} = 50$ and mesh grading were used to compute these examples, which allocate ~ 0.1 MB memory. The relative error calculated from the energy balance for absorption gratings is $\sim 10^{-4}$. The average time taken up by one point on a portable IBM workstation ThinkPad R50p with an Intel Pentium M 1.7-GHz processor and 2 GByte of RAM is ~ 0.1 s only when operating on Linux (kernel 2.6.17).

B. PBGs with high-conductive rods supporting waveguide modes

As demonstrated in the previous example, owing to the existence of surface plasmon resonance, even a single-grating structure could almost totally transmit TM polarization (Figs. 3–6). One can exclude the influence of plasmon surface waves using a grating structure in TE polarization for which plasmons cannot propagate and investigate the role of waveguide modes and Fabry-Perot resonances.

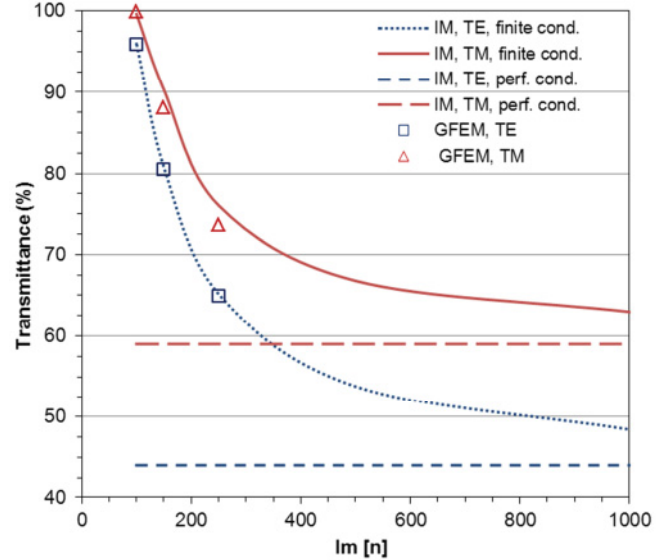


FIG. 7. (Color online) TE and TM transmittances of a $d = 10$ mm grating with high-conductive rectangular rods of 7×1 mm^2 cross section, which are embedded in a matrix with $n_0 = 3.47$, $N - 1 = 2$, $H = 1$ mm, and $L = 0$, are plotted vs $\text{Im}[n]$. Calculations were performed for normal incidence at $\lambda = 15.24$ mm.

Figure 7 displays transmission TE and TM spectra for PBGs with high-conductive lossless ($\text{Re}[n_2] = 0$) rectangular rods of 7×1 mm^2 with $d = 10$ mm embedded in a matrix with $n_1 = 3.47$ for $N - 1 = 2$, $H = 1$ mm, and $L = 0$ at $\lambda = 15.24$ mm. The outermost media have refractive index $n_{0,3} = 1$. Very similar spectra were calculated in Fig. 10 a in Ref. [39] by the CWM for TE polarization and $\text{Im}[n_2] = 250$ only. In addition, the efficiency simulation data based on the present IM were cross-checked in both polarization states against the rigorous generalized finite element method (GFEM) [40], in order to verify the reliability of the results obtained. The grating efficiencies calculated with two different approaches mentioned above are in good agreement for all compared $\text{Im}[n_2]$ data. Obviously enough, the difference between the transmittance values calculated by the two independent codes is bigger for the TM polarization state and higher $\text{Im}[n_2]$. So the applicability of the IM and GFEM to analyze both TE and TM diffraction on such PBGs for high values of the imaginary part of the refractive index of rods is demonstrated. One can also compare the absolute efficiencies of this example with values predicted by the perfect-conductivity model (Fig. 7). The asymptotic transmittance data calculated using that model are $\sim 44\%$ (TE) and $\sim 59\%$ (TM). Interestingly, even at the very high value of $\text{Im}[n_2] = 1000$, the results obtained for the finite-conductivity model differ significantly from those obtained for the perfect-conductivity model.

For this very-hard-to-solve example we examine the convergence rate and the accuracy of the prediction of reflection and transmission energies and absorption with respect to \mathcal{N} . For the efficiency convergence testing, the magnitude of computational errors cannot be reliably deduced from accuracy criteria based on a single computation such as the energy balance or the inverse radiation condition tests. For this purpose, comparative studies should be used, i.e., \mathcal{N}

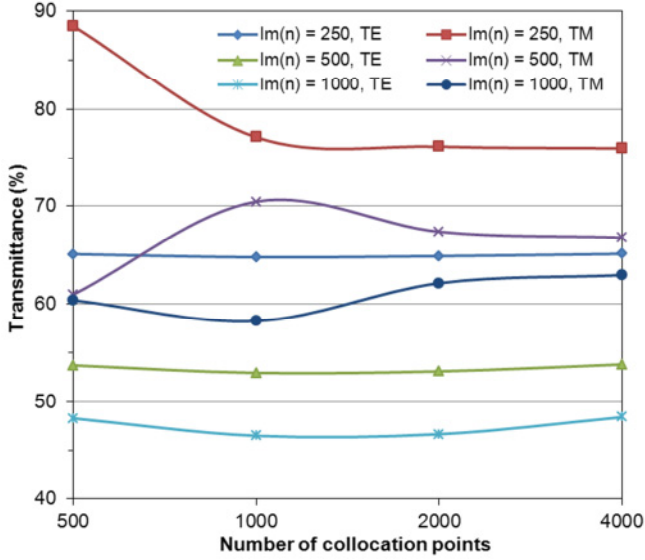


FIG. 8. (Color online) TE and TM transmittances of a $d = 10$ mm grating with high-conductive rectangular rods of 7×1 mm² cross section, which are embedded in a matrix with $n_0 = 3.47$, $N - 1 = 2$, $H = 1$ mm, and $L = 0$, are plotted vs the number of collocation points. Calculations were performed for normal incidence at $\lambda = 15.24$ mm.

doubling [19]. As shown in Fig. 8, the IM transmittance values for $\text{Im}[n_2] = 250$ and $\text{Im}[n_2] = 500$ stabilize, and the convergence starts at $\mathcal{N} = 500$ (TE) and $\mathcal{N} = 1000$ (TM) and is achieved with a high accuracy at $\mathcal{N} = 1000$ (TE) and $\mathcal{N} = 2000$ (TM). The absolute differences between the values calculated for $\mathcal{N} = 1000$ and $\mathcal{N} = 4000$ in the transmission energies for $\text{Im}[n_2] = 250$ are 0.00353 for TE polarization and 0.0111 for TM polarization. Note that the energy balance errors are $\sim 10^{-5}$ and $\sim 10^{-6}$ for these values of \mathcal{N} , respectively. However, transmittance values for the hard case of $\text{Im}[n_2] = 1000$ stabilize at $\mathcal{N} = 4000$ only. Thus, the convergence rate is high enough, taking into account the very difficult cases tested.

The computation time for a point calculated with ($\mathcal{N} = 2000$) is ~ 30 s on the above-mentioned PC, and the required RAM is ~ 1 GB. In this case the use of graded meshes gave the most accurate results compared with data obtained by applying other computational options.

C. PBGs with dielectric rods supporting Bragg diffraction

In this example we consider numerically some diffraction properties of nonabsorbing PBGs with dielectric rods. The influence of the geometry and number of crystal layers, the shape of the rods, the filling ratio, the index of refraction of materials, and the polarization and diffraction angles of light can be investigated for this type of PBGs. The vital role of the filling ratio, refractive index, and polarization was demonstrated for classical diffraction [2,34]. Here we demonstrate, as an example of the possibilities of developed software, the vital role of the filling ratio and polarization for conical diffraction.

Figures 9 and 10 display spectral transmission for PBG circular rods with $d = 1 \mu\text{m}$ and $n_2 = 2$ embedded in a

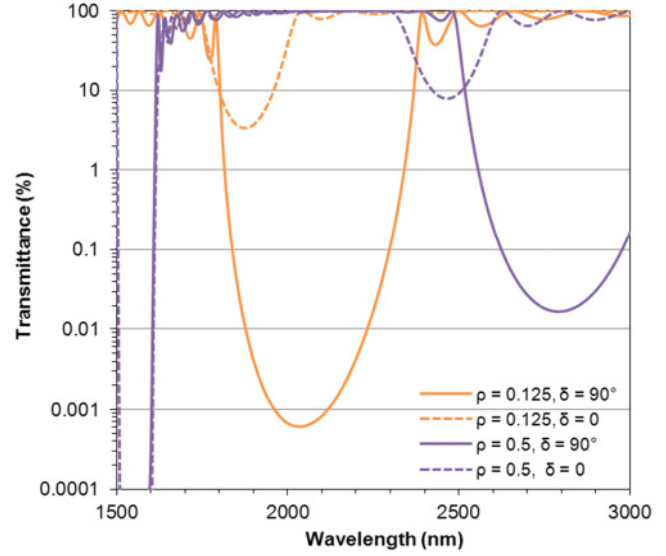


FIG. 9. (Color online) Calculated transmission spectra of a $d = 1 \mu\text{m}$ grating with dielectric circular rods with $n_2 = 3.47$ and filling ratio ρ , embedded in a vacuum with $N - 1 = 15$, $H = 0.866 \mu\text{m}$, and $L = 0.5 \mu\text{m}$, are plotted vs the wavelength of incidence radiation with $\theta = 0$, $\phi = 0$ (classical diffraction), and polarization angle δ .

vacuum at filling ratios of 0.125 and 0.5 for $N - 1 = 15$, $H = 0.866 \mu\text{m}$, and $L = 0.5 \mu\text{m}$ (hexagonal crystal geometry) for $\theta = 0$, $\psi = 0$, and $\delta = 90^\circ$ (TE or s polarization) or $\delta = 0^\circ$ (TM or p polarization). Figure 9 shows in-plane diffraction efficiencies ($\phi = 0$) and similar transmittance data computed in Ref. [34] by the IM (Figs. 6 and 11 in Ref. [34]). In Fig. 10, for off-plane diffraction $\phi = 30^\circ$ and this is an additional parameter compared with the classical diffraction case.

For both in-plane and off-plane examples there is a very different behavior in diffraction properties for the TE and TM polarizations of the incident radiation, especially for high filling ratios. Compared with the respective curves obtained

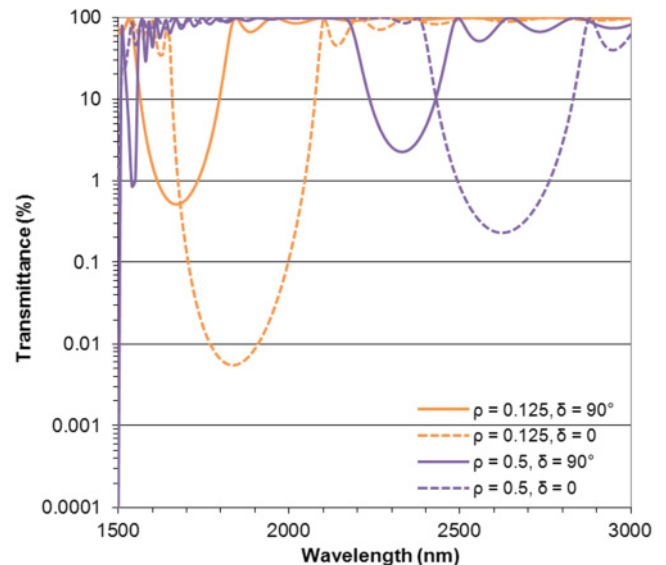


FIG. 10. (Color online) The same as Fig. 9, but for $\phi = 30^\circ$ (conical diffraction).

in Figs. 9 and 10, it emerges that for s -polarized light the centers of the conical diffraction gaps have shifted significantly to lower wavelengths and the widths and depths of the gaps have decreased considerably. In contrast to this behavior, for p -polarized light the centers of the conical diffraction gaps compared with the in-plane ones have shifted a little bit in opposite directions and the widths and depths of these gaps have increased considerably. The vital importance of the azimuthal angle ϕ as well as the incidence polarization has become evident even for a low filling ratio (0.125), however, they are more important for a high filling ratio (0.5). Thus, using the conical diffraction for dielectric PBGs gives additional control parameters which significantly affect Bragg diffraction and existing PBGs.

Only $\mathcal{N} = 50$ without mesh grading is required to compute this example, which allocates ~ 0.2 MB memory. The relative error calculated from the energy balance for nonabsorption gratings is $\sim 10^{-4}$. The average time taken up by one point on the above-mentioned PC is ~ 1 s.

V. SUMMARY AND CONCLUSIONS

The multilayer integral-equation-based method is proposed to calculate diffraction properties of PBGs with separated boundaries. It is possible to determine the diffraction-field amplitudes by computing the scattering matrices separately for various grating boundary profiles including dielectric, absorbing, and high-conductive rods working in any wavelength range. Computation of the matrices is based on the solution of a 2×2 system of singular integral equations at each interface between two different materials. The discretization of the integral equation system and the factorization of the discrete matrices (which takes the major computing time for one-boundary problems as well) have to be performed only once in order to compute these matrices for each boundary profile. It turns out that, due to the high convergence rate, a small number of collocation points per boundary combined with a high convergence rate can provide an adequate description of the dependence on diffracted energy of very different PBGs illuminated at arbitrary incident and polarization angles.

In the present numerical analysis of the optical response of PBGs, a significant impact of rod shapes on diffraction supporting polariton-plasmon excitation, particularly in the vicinity of resonances and at high filling ratios, has been investigated. The most sensitive rod shapes are rectangular and triangular due to their lower symmetry and special resonance features connected with edges. The diffracted energy response calculated vs the array-cell geometry parameters was found to vary from a few up to a few hundred percent. The influence of other types of anomalies (i.e., waveguide anomalies, cavity modes, Fabry-Perot and Bragg resonances, Rayleigh orders, etc.), conductivity, and polarization states has been demonstrated. Unexpectedly, the results obtained for the finite-conductivity model of PBGs with high-conductive lossless ($\text{Re}[n_2] = 0$) rectangular rods at very high values of $\text{Im}[n_2]$ differ significantly from those obtained for the perfect-conductivity model. The vital role of conical diffraction ($\phi \neq 0$) as well as incident polarization has been demonstrated for PBGs with dielectric circular rods supporting Bragg diffraction at different filling ratios. Thus, the rod and diffraction geometries, conductivity, and polarization cannot be ignored in many sensitive cases, and simple and inaccurate theories cannot be applied to the design and analysis of such complex PBGs. The multilayer conical solver developed and tested is found to be very accurate and fast for solving PBG diffraction problems with high-conductive rods of arbitrary shapes, in particular, with real boundary profiles, the case that should be studied experimentally. Due to the good convergence, the considered IM can be extended to handle 3D PBGs (2D multilayer diffraction gratings), which will be addressed in future publications.

ACKNOWLEDGMENTS

The authors are indebted to Andreas Rathsfeld (Weierstrass Institute for Applied Analysis and Stochastics, Germany) for the information provided and fruitful testing. Helpful discussions with Bernd Kleemann (Carl Zeiss AG, Germany) and Sergey Sadov (Memorial University of Newfoundland, Canada) are greatly appreciated.

-
- [1] R. Petit (ed.), *Electromagnetic Theory of Gratings* (Springer, Berlin, 1980).
 - [2] K. Yasumoto (ed.), *Electromagnetic Theory and Applications for Photonic Crystals* (Taylor & Francis, Boca Raton, FL, 2006).
 - [3] E. G. Loewen and E. Popov, *Diffraction Gratings and Applications* (Marcel Dekker, New York, 1997).
 - [4] M. Neviere and E. Popov, *Light Propagation in Periodic Media: Differential Theory and Design* (Marcel Dekker, New York, 2003).
 - [5] S. G. Johnson and J. D. Joannopoulos, *Photonic Crystals: The Road from Theory to Practice* (Springer, New York, 2002).
 - [6] S. G. Johnson and J. D. Joannopoulos, *Opt. Express* **8**, 173 (2001).
 - [7] G. Kobidze, B. Shanker, and D. P. Nyquist, *Phys. Rev. E* **72**, 056702 (2005).
 - [8] A. Christ, T. Zentgraf, J. Kuhl, S. G. Tikhodeev, N. A. Gippius, and H. Giessen, *Phys. Rev. B* **70**, 125113 (2004).
 - [9] M. G. Moharam and T. K. Gaylord, *J. Opt. Soc. Am.* **71**, 811 (1981).
 - [10] B. Kleemann, A. Mitreiter, and F. Wyrowski, *J. Mod. Opt.* **43**, 1323 (1996).
 - [11] E. Popov, B. Chernov, M. Neviere, and N. Bonod, *J. Opt. Soc. Am. A* **21**, 199 (2004).
 - [12] B. Guizal, H. Yala, and D. Felbacq, *Opt. Lett.* **34**, 2790 (2009).
 - [13] E. Popov, M. Neviere, B. Gralak, and G. Tayeb, *J. Opt. Soc. Am. A* **19**, 33 (2002).
 - [14] M. A. Gilman, S. Yu. Sadov, A. S. Shamaev, and S. I. Shamaev, *J. Commun. Technol. Electron.* **45**, S229 (2000).
 - [15] V. A. Soifer (ed.), *Methods for Computer Design of Diffractive Optical Elements* (Wiley, New York, 2002).

- [16] A. Rathsfeld, G. Schmidt, and B. H. Kleemann, *Commun. Comput. Phys.* **1**, 984 (2006).
- [17] L. I. Goray and S. Y. Sadov, in *Diffraction Optics and Micro-Optics*, OSA Trends in Optics and Photonics Series Vol. 75 (Optical Society of America, Washington, DC, 2002), pp. 365–379.
- [18] [<http://www.pcgrate.com>] (2012).
- [19] L. I. Goray and G. Schmidt, *J. Opt. Soc. Am. A* **27**, 585 (2010).
- [20] B. H. Kleemann and J. Erxmeyer, *J. Mod. Opt.* **51**, 2093 (2004).
- [21] L. I. Goray and J. F. Seely, *Appl. Opt.* **41**, 1434 (2002).
- [22] L. I. Goray, J. F. Seely, and S. Yu. Sadov, *J. Appl. Phys.* **100**, 094901 (2006).
- [23] L. I. Goray, *J. Appl. Phys.* **108**, 033516 (2010).
- [24] Y. Wu and Y. Y. Lu, *J. Opt. Soc. Am. A* **28**, 1191 (2011).
- [25] G. Schmidt, in *Around the Research of Vladimir Maz'ya II. Partial Differential Equations* (Springer, New York, 2010), p. 337.
- [26] L. I. Goray, *Waves Random Media* **20**, 569 (2010).
- [27] G. Schmidt, *Appl. Anal.* **82**, 75 (2003).
- [28] J. Seely, B. Kjornrattanawanich, L. Goray, Y. Feng, and J. Bremer, *Appl. Opt.* **50**, 3015 (2011).
- [29] G. Schmidt and B. H. Kleemann, *J. Mod. Opt.* **58**, 407 (2011).
- [30] J. M. Taboada, J. Rivero, F. Obelleiro, M. G. Araujo, and L. Landesa, *J. Opt. Soc. Am. A* **28**, 1341 (2011).
- [31] L. I. Goray and G. Schmidt, in *Days on Diffraction 2009, Proceedings of the International Conference, St. Petersburg, Russia, May 26–29* (IEEE, St. Petersburg, 2010), pp. 92–97.
- [32] L. I. Goray, *Proc. SPIE* **7390**, 73900V (2009).
- [33] L. Li, *J. Opt. Soc. Am. A* **13**, 1024 (1996).
- [34] D. Maystre, *Pure Appl. Opt.* **3**, 975 (1994).
- [35] S. A. Schelkunoff, *Bell Syst. Tech. J.* **17**, 17 (1938).
- [36] A. Christ, Y. Ekinici, H. H. Solak, N. A. Gippius, S. G. Tikhodeev, and O. J. F. Martin, *Phys. Rev. B* **76**, 201405 (2007).
- [37] P. B. Johnson and R. W. Christy, *Phys. Rev. B* **6**, 4370 (1972).
- [38] E. D. Palik (ed.), *Handbook of Optical Constant of Solids* (Academic, Orlando, FL, 1985).
- [39] E. Popov, S. Enoch, G. Tayeb, M. Neviere, B. Gralak, and N. Bonod, *Appl. Opt.* **43**, 999 (2004).
- [40] J. Elschner, R. Hinder, A. Rathsfeld, and G. Schmidt, DIPOG homepage [<http://www.wias-berlin.de/software/DIPOG>] (2012).